THE JOURNAL OF BIOLOGICAL CHEMISTRY
Vol. 271, No. 28, Issue of July 12, pp. 16703–16711, 1996

Printed in U.S.A.

Determination of the Structure of the N-terminal Splice Region of the Cyclic AMP-specific Phosphodiesterase RD1 (RNPDE4A1) by ^{1}H NMR and Identification of the Membrane Association Domain Using Chimeric Constructs*

(Received for publication, January 30, 1996, and in revised form, April 18, 1996)

K. John Smith‡, Grant Scotland§, James Beattie¶, Ian P. Trayer‡, and Miles D. Houslay§‖

From the §Molecular Pharmacology Group, Division of Biochemistry and Molecular Biology, Davidson Building, Institute of Life and Biomedical Sciences, University of Glasgow, Glasgow G12 8QQ, Scotland, the ‡School of Biochemistry, University of Birmingham, Edgbaston, Birmingham B15 2TT, and the ¶Hannah Research Institute, Ayr KA6 5HL, Scotland, United Kingdom

A 25-residue peptide representing the membrane targeting N-terminal splice region of the cyclic AMP phosphodiesterase RD1 (RNPDE4A1) was synthesized, and its structure was determined by ^{1}H NMR. Two independently folding helical regions were identified, separated by a highly mobile "hinge" region. The first helical region was formed by an N-terminal amphipathic α-helix, and the second consisted of multiple overlapping turns and contained a distinct compact, hydrophobic, tryptophan-rich domain (residues 14–20). Chimeric molecules, formed between the N-terminal region of RD1 and the soluble bacterial protein chloramphenicol acetyltransferase, were used in an *in vitro* system to determine the features within the splice region that were required for membrane association. The ability of RD1-chloramphenicol acetyltransferase chimera to become membrane-associated was not affected by deletion of any of the following regions: the apolar section (residues 2–7) of the first helical region, the polar part of this region together with the hinge region (residues 8–13), or the polar end of the C-terminal helical region (residues 21–25). In marked contrast, deletion of the compact, hydrophobic tryptophan-rich domain (residues 14–20) found in the second helical region obliterated membrane association. Replacement of this domain with a hydrophobic cassette of seven alanine residues also abolished membrane association, indicating that membrane-association occurred by virtue of specific hydrophobic interactions with residues within the compact, tryptophan-rich domain. The structure of this domain is well defined in the peptide, and although the region is helical, both the backbone and the distribution of side chains are somewhat distorted as compared with an ideal α-helix. Hydrophobic interactions, such as the "stacked" rings of residues Pro^{14} and Trp^{15}, stabilize this domain with the side chain of residue Leu^{16} adopting a central position, interacting with the side chains of all three tryptophan residues 15, 19, and 20. These bulky side chains thus form a hydrophobic cluster. In contrast, the side chain of residue Val^{17} is relatively exposed, pointing out from the opposite "face" of the peptide. Although it appears that this compact, tryptophan-rich domain is responsible for membrane association, at present the target site and hence the specific interactions involved in membrane targeting by the RD1 splice region remain unidentified.

cAMP serves to influence a variety of cellular processes (1). The sole means of degrading this key second messenger within cells is through hydrolysis to 5′-AMP, which is achieved by a family of cAMP phosphodiesterases (PDE) (2–4).[1] At least five distinct families encode enzymes that display this activity, each of which exhibits distinct regulatory properties (2–4). Indeed, PDEs appear to provide a point of "cross-talk" between the cAMP signaling system and most, if not all, other signaling systems, suggesting that these enzymes may play a key role in signal integration. There is also considerable evidence to suggest that the functioning of cAMP within various cells may be compartmentalized (5–7). The molecular machinery that might allow for this includes the functional targeting of type-II cAMP-dependent protein kinase (protein kinase A) to specific cellular membranes through interaction with a family of membrane-associated protein kinase A binding proteins (5–7). Coupled to this are the observations that degradation of cAMP can be compartmentalized, as specific PDEs are also membrane-associated (8–10). The PDE4 cAMP-specific PDEs provide clear examples of both cytosolic and membrane-associated PDEs (11, 12). This family is encoded by four separate genes found on three different chromosomes (13–15) with additional complexity derived from alternative splicing (16–18). The PDE4A gene family in rat has at least three members (17, 18), which are RD1 (RNPDE4A1), RPDE-6 (RNPDE4A), and RPDE-39 (RNPDE4A6). These enzymes are differentially expressed in various tissues and are formed by 5′ alternative splicing to yield proteins with distinct N-terminal regions (11, 12, 17). The engineered expression of the common "core" PDE4A gene product produces a highly active cytosolic protein (9, 12, 19). In contrast, the splice variant RD1 is found exclusively associated

* This work was supported in part by funds from the Medical Research Council (United Kingdom) (to M. D. H.), by equipment grants from the Wellcome Trust and the Scottish Home and Health Department (to M. D. H.), and funds from the the Wellcome Trust (to K. J. S.). The costs of publication of this article were defrayed in part by the payment of page charges. This article must therefore be hereby marked "*advertisement*" in accordance with 18 U.S.C. Section 1734 solely to indicate this fact.

The nucleotide sequence(s) reported in this paper has been submitted to the GenBank™/EBI Data Bank with accession number(s) M26715.

The atomic coordinates and structure factors (codes 1LOI and R1LOIMR) have been deposited in the Protein Data Bank, Brookhaven National Laboratory, Upton, NY.

‖ To whom correspondence should be addressed. Tel.: 44-141-330-5903; Fax: 44-141-330-4620; E-mail: gbca29@udcf.gla.ac.uk.

[1] The abbreviations used are: PDE, cyclic 3′,5′-AMP phosphodiesterase; CAT, chloramphenicol acetyltransferase; PCR, polymerase chain reaction; TFE, 2,2,2-trifluoroethanol; TOCSY, total correlation spectroscopy; NOESY, nuclear Overhauser enhancement spectroscopy; NOE, nuclear Overhauser effect; d_3, fully deuterated.

with membranes (12, 19), whereas both RPDE6 (12) and RPDE39 (11) are expressed as both soluble and particulate-associated species. These unique N-terminal regions not only define intracellular targeting, but they also profoundly reduce catalytic activity (V_{max}) and alter thermostability (9, 12, 19).

That the N-terminal splice region of RD1 (18) encodes a structure able to target an essentially soluble core PDE to the membrane fraction (9, 19) is supported by our observation (20) that "in-frame" chimera formed from this region of RD1 and CAT confers exclusive membrane-association upon this normally cytosolic, bacterial protein. Here we employ deletion analysis of RD1-CAT chimera to identify which of the distinct structural domains, identified using ^{1}H NMR analysis of a 25-residue peptide encompassing the N-terminal splice region of RD1, is responsible for determining membrane association.

MATERIALS AND METHODS

GeneAmp™ PCR Reagent kit was purchased from Perkin-Elmer. Restriction and modifying enzymes, TnT™ SP6 Coupled Reticulocyte Lysate System, Wizard™ PCR, and Miniprep and Maxiprep systems were from Promega. Qiaex PCR purification kit was from Hybaid Ltd. *Taq* DyeDeoyx™ Terminator Cycle Sequencing kits were from Applied Biosystems. [^{14}C]Chloramphenicol (54 mCi/mmol), [^{35}S]methionine (50 mCi/mmol), ^{14}C-labeled protein molecular weight markers, and ECL Western blot detection reagents were from Amersham International plc. All other chemicals and reagents were of the highest quality available (Sigma). Plasmid pSVL-RD1 containing RD1 has been described previously (9). Plasmid pSV.SPORT was from Life Technologies Inc. PCR and sequencing primers were designed with the Gene Jockey program (Biosoft) (21) and synthesized on an Applied Biosystems model 381A.

Peptide Synthesis—A peptide representing the N-terminal first 25 amino acids of RD1 (MPLVDFFCETCSKPWLVGWWDQFKR) was synthesized via automated Fmoc ((fluorenyl)methoxycarbonyl) chemistry on an Applied Biosystems 431A peptide synthesizer. The peptide amide was synthesized on a Rink Amide MBHA resin (Nova Biochem; 01-64-0037). Amino acid residues were used with following side chain protection: D,E,T,S-*t*-butyl; C,Q-trityl; K-Boc; and R-Pmc. Cleavage of peptide from the resin, with simultaneous deprotection of side chains, was done with 10 ml of trifluoroacetic acid containing 0.5 ml of H_20, 0.5 ml of thioanisole, and 0.25 ml of ethanedithiol. Crude peptide was precipitated in ice-cold diethyl ether, dried in a stream of N_2, and lyophilized from 10% acetic acid. Purification was by semi-preparative reverse phase chromatography (Vydac C18 column, 25 × 1 cm) using a 0–70% acetonitrile gradient at a flow rate of 5 ml/min over 76 min. Peptide identity and purity was confirmed by matrix-assisted laser desorption ionization mass spectroscopy and Edman sequencing.

NMR Spectroscopy—^{1}H NMR experiments were carried out on a Bruker AMX500 spectrometer using standard phase sensitive two-dimensional pulse sequences. Two-dimensional experiments were acquired with 2048/2K data points in F2, using a sweep width of 5500 Hz, and with 448 rows in F1. For TOCSY and COSY experiments 16 transients were acquired, and for NOESY experiments 80 transients were acquired. TOCSY experiments used an MLEV-17 mixing pulse of 60-ms duration (10 kHz spin locking field).

The NOESY experiments were collected with mixing times of 50, 100, and 200 ms. Very weak presaturation was applied to the water resonance both during the relaxation delay (1.5 s) and also during the mixing time of the NOESY experiments.

TOCSY, NOESY, and COSY spectra for assignment were collected on 7 mM solutions of peptide in the presence of 6–8 mM dithiothreitol, at both pH 6.0 in 50% d_3 TFE/50% H_2O (v/v, 300 K) and at pH 3.9 50% d_3 TFE/50% H_2O (v/v, 304 K). The addition of dithiothreitol eliminated the possibility of inter- and intramolecular disulfide bridge formation. Sequential NOEs were identified along the whole of peptide backbone, enabling proton resonances to be assigned in a quite straightforward fashion. The unambiguous identity of certain NOE cross-peaks was confirmed taking advantage of pH- and temperature-dependent shifts between different spectra.

In order to detect backbone hydrogen bonding in the peptide, the rates of movement of chemical shifts with changes in temperature were followed in TOCSY spectra at temperatures between 285 and 311 K at both pH 4.1 and 6.0 with essentially no difference seen between the two data sets. Temperature shift coefficients were determined from the slope of a linear plot of temperature against chemical shift. Inter-proton distances were estimated from NOESY experiments by integration to yield cross-peak volumes in the 200-ms NOESY spectrum (all cross-peaks were also seen at 100 ms of mixing time). Cross-peaks were grouped into five classes between strong and very weak (strong and medium NOEs were allocated the same distance constraint values in calculations).

The peptide structure was determined using XPLOR 3.1 (22) using a protocol in which certain atoms of each residue were embedded using the distance geometry routine (atoms CA, HA, N, HN, C, CB*, CG*, dg_sub_embed protocol). The remaining atoms were placed by template fitting, and then the atomic co-ordinates were allowed to evolve under the applied NOE distance constraints during a series of high temperature simulated annealing steps (dgsa and refine protocols). From the 100 calculated co-ordinate sets started, half were discarded (wrong handedness in the distance geometry routine). The final structures were produced by minimizing the averaged co-ordinates produced over the last 4 ps of a 5-ps low temperature simulated annealing trajectory. 25 structures were then chosen with no violations of the applied NOE constraints greater than 0.4 Å for analysis. To aid analysis, a mean structure was calculated by simultaneously refining these 25 structures in a high temperature simulated annealing protocol and applying an additional constraint tending to minimize the RMS difference between the aligned co-ordinates (NCS restraints applied individually to the regions Met^1–Cys^{11}, Cys^{11}–Pro^{14}, and Pro^{14}–Arg^{25}). It was not found necessary to include constraints for hydrogen bonds in any calculation. The pattern of hydrogen bond donors, indicated by changes in the rate of change in chemical shift of the backbone amides with changes in pH, was consistent with the calculated structures. There were no significant differences between the NOEs observed at pH 3.9 and 6.0, indicating that the structures were very similar.

NMR data collected in water alone were of poor quality because of limited solubility of the peptide (less than 0.5 mM at pH 4 and lower at pH 6). The data implied that the problem was nonpolar aggregation at residues Leu^3, Phe^6, and Phe^7 in the N-terminal amphipathic α-helix. However, in the water/TFE mixture intermolecular interactions were eliminated (*e.g.*, there was no change in line width or chemical shift as concentrations were decreased). Trifluoroethanol was chosen as a co-solvent with water in this study because of its ability to reduce hydrophobic interactions between peptides (23) and because of the enhancement of secondary structure for small peptides in solution, see *e.g.*, Refs. 24 and 25.

Construction of Deletion Mutations—Various mutations were generated within the 25-amino acid N-terminal region of RD1 by a modification of the method of overlapping extension mutagenesis described by Ho *et al.* (26). Primer pairs used were: GSOL17, 5′-GGTCGACTCTAGAATGTGCGAGACCTGC-3′, and GSOL18, 5′-GCAGGTCTCGCACATTCTAGAGTCGACC-3′ to generate deletion ΔP2-F7 (inclusive); GSOL27, 5′-GACTTCTTCCCCTGGCTGG-3′, and GSOL28, 5′-CCAGCCAGGGGAAGAAGTC-3′ to generate deletion ΔC8-K13 (inclusive); GSOL36, 5′-CCTGCTCCAAGGACCAGTTCAAAAGG-3′, and GSOL37, 5′-CCTTTTGAACTGGTCCTTGGAGCAGG-3′ to generate deletion ΔP14-W20 (inclusive); GSOL38, 5′-GCTGGTGGATGCTGAACC-3′, and GSOL39, 5′-GGTTCAGCATCCACCAGC-3′ to generate deletion ΔD21-R25 (inclusive); and GSOL62, 5′-CCTGCTCCAAGGCAGCAGCAGCAGCAGCAGACCAGTTCAAAAGG-3′, and GSOL62, 5′-CCTTTTGAACTGGTCTGCTGCTGCTGCTGCTGCCTTGGAGCAGG-3′ were used to replace P14-W20 (inclusive) of pGS7 with a cassette of seven alanine residues through the generation of plasmid pGS22. Primers GSOL10 (5′-CCAGTCACGACGTTGTAA-3′) and GSOL15 (5′-GGCTCCTCGAGCTTCCAGTGTGT-3′) were used as the sense and antisense primers, respectively, for each mutation-generating PCR reaction.

Using plasmid pGS4 (20) as template DNA, the following reaction conditions were used: 1 μg of template DNA, 25 pmol of each primer, 0.2 mM each dNTP, 50 mM KCl, 10 mM Tris-HCl, pH 9.0, 0.1% Triton X-100 (v/v), 1.5 mM $MgCl_2$, and 2.5 units of *Taq* polymerase 1 in a final volume of 50 μl with a mineral oil overlay. The reaction was subjected to the following conditions in a Techne PHC-3 thermocycler: denaturation for 1′ at 94 °C, annealing for 2′ at 37 °C, and extension for 3′ at 72 °C for one cycle followed by denaturation for 1′ at 94 °C, annealing for 2′ at 50 °C, and extension for 3′ at 72 °C for 30 cycles. Upon completion of the primary PCR reactions, samples were extracted once with an equal volume of chloroform to remove mineral oil before electrophoresis through a 1.75% low gelling temperature agarose gel. Fragments were identified by ultraviolet transilluminator and excised, and a small fraction (~ 5 μl of each band) was mixed together and subjected to the same reaction conditions as was done previously but in the absence of the complementary mutagenic primers. When a second round of PCR

was carried out under to the same conditions as done initially, but in the presence only of primers GSOL10 and GSOL15, a hybrid PCR product was generated containing the mutation of interest. Annealing of the two primary PCR products was facilitated by the complementary nature of the 3′ ends of the fragments generated during the primary reaction. Upon completion the reactions were extracted with an equal volume of chloroform as before and digested with restriction enzymes *Xba*I (12 units) and *Xho*I (8 units) in 6 mM Tris-HCl (final pH 7.9), 150 mM NaCl, 6 mM $MgCl_2$, and 1 mM dithiothreitol for 2 h. at 37 °C. Digested fragments were recovered from 1.75% low gelling temperature agarose gels as before and substitute for the wild type RD1 N-terminal fragment of pGS7 (20) to create the plasmids pGS10, pGS15, pGS17, pGS18, and pGS22 containing the deletions/substitution ΔP2-F7, ΔC8-K13, ΔP14-W20, ΔD21-R25, and the alanine cassette substitution Ala^{7} (14–20), respectively.

Membrane Association Assay—This was carried out as described previously by us in some detail (20). Here we used a chimera formed between the N-terminal first 100 amino acids of RD1 fused, in frame, to the N terminus of CAT (20). This has been shown (20) to become associated with membranes in exactly the same way as the 1-25RD1-CAT chimera. The choice of the larger species was made because it facilitated performing the molecular engineering analyses, which otherwise would have been extremely difficult to do on the nucleotides encoding 1-25RD1 due to the small size of the fragment. The TnT®-coupled transcription/translation system (Promega) was used to generate mature proteins from plasmid DNA. Post-translation duplicate aliquots were taken, and either TEN buffer or TEN buffer containing COS cell membranes was added. Samples were incubated at 37 °C for 30 min and then centrifuged to yield a soluble fraction and a membrane pellet, which was subsequently washed (20). All samples were adjusted to give equal volumes prior to SDS-polyacrylamide gel electrophoresis and visualization on a PhosphorImager.

RESULTS AND DISCUSSION

The N-terminal splice region of the cyclic AMP-specific phosphodiesterase RD1 is formed by the N-terminal first 23 amino acids (17). Here we provide a ^{1}H NMR structural analysis of a synthetic peptide, which represents the N-terminal first 25 amino acids of RD1 and thus encompasses all of this region. The ability of distinct domains formed within this region to confer membrane association was then studied using deletion analysis performed on chimeric species formed from the N-terminal first 100 amino acids of RD1 linked to the soluble reporter protein CAT (20).

The NMR-derived Structure of the 1-25 RD1—Sections from the NOESY spectrum used in the structure determination are shown in Fig. 1. A total of 406 NOEs were identified, 221 of these were inter-residue NOEs with 87 separated by more than one residue and 57 separated by more than two residues. A summary of these NOEs, which were used as distance restraints in the structure calculation, is shown in Fig. 2. A significant population of α-helix in the peptide structure was indicated by the NMR study, and this was confirmed by CD spectroscopy. In 50% d_3TFE/50% H_2O (v/v), 27% α-helix was detected at pH 3.9, and 33% α-helix was detected at pH 7.0. In water alone, only 4 and 6% α-helix was found at pH 3.9 and 7.0, respectively (data not shown).

The region Leu^{3}–Cys^{11} forms an amphipathic α-helix with the nonpolar residues Leu^{3}, Val^{4}, Phe^{6}, and Phe^{7} along one side of the helical cylinder (Figs. 3 and 4). As expected, the first two residues in the peptide form a "frayed" end with little conformational preference. The helical conformation of the peptide backbone is indicated by the large $d_{NN}(i,i+1)$ NOEs for all residues (present after 50 ms of mixing time and so not a result of spin diffusion) and by medium-range connectivities of the type $d_{\alpha N}(i,i+3)$ for residues Leu^{3}–Phe^{6}, Val^{4}–Phe^{7}, Asp^{5}–Cys^{8}, Phe^{6}–Glu^{9}, and Cys^{8}–Cys^{11} (27). In addition, the expected weaker connectivities, $d_{\alpha N}(i,i+4)$ (residues Val^{4}–Cys^{8} and Asp^{5}–Glu^{9}), $d_{\alpha N}(i,i+2)$ (residues Pro^{2}–Val^{4} and Asp^{5}–Phe^{7}), and $d_{NN}(i,i+2)$ (residues Leu^{3}–Asp^{5}, Val^{4}–Phe^{6}, Asp^{5}–Phe^{7}, Phe^{6}–Cys^{8}, and Cys^{8}–Thr^{10}) were also seen. A substantial population of α-helix with well ordered side chains is confirmed by $d_{\alpha\beta}(i,i+3)$ connectivities (residues Leu^{3}–Phe^{6}, Val^{4}–Phe^{7}, Phe^{6}–Glu^{9}, Cys^{8}–Cys^{11}). Although some NOEs may have been obscured by spectral overlap, more than sufficient were observed to clearly define the α-helix. The principle contributors to helical stability are the $i,i+4$ hydrogen bonds. The hydrogen bonds indicated in the calculated structures were 4CO-8HN, 5CO-9HN, and 6CO-10HN and such donors confirmed by the slow rate of backbone amide exchange in residues Cys^{8}, Glu^{9}, and Thr^{10} (<2 ppb/K). The α-helical region appears to end with a 3_{10}-helical hydrogen bond, $Cys^{8}{}_{C=O}$ to $Cys^{11}{}_{HN}$, corresponding to a reduced exchange rate at the backbone amide of residue Cys^{11}. Additional stabilization of the helix arises from the electrostatic interaction of the charged N terminus $Mey^{1}{}_{NH3+}$ with the side chain of Asp^{5} (the NOE $d_{\beta N}(i,i+3)$, for residues Met^{1}–Val^{4} providing supporting evidence for this ion pair). This interaction may offset the destabilizing effect of the charged N terminus upon the helical dipole (28, 29).

Examination of the distribution of NOEs shown in Fig. 2 indicates that very few restraints were identified in the region Cys^{11}–Pro^{14}. This area has the most poorly defined backbone and side chain conformation in the calculated structure, and it may correspond to region of high mobility, forming a "hinge" in the splice region of RD1. This point is illustrated by the aligned calculated structures shown in Fig. 3 in which either the C terminus or the N terminus needs to be aligned independently. The backbone Ø/Ψ plot is particularly poorly defined at residues Cys^{11} and Ser^{12}. The reason for termination of the α-helix following residue Cys^{11} is not clear, although the presence in this area of so many consecutive residues with side chains capable of hydrogen bonding with the peptide backbone (*e.g.*, Thr^{10}, Cys^{11}, or Ser^{12}) might be expected to result in the interruption of the α-helix by competition with the helical backbone hydrogen bonds (30). Among the few NOEs observed over this region, there are indications of an irregular β-turn between residues Cys^{11}–Pro^{14} (*e.g.*, located by the medium strength NOE $Ser^{12}{}_{\alpha H}$–$Pro^{14}{}_{H\delta}$). In the absence of other NOEs, there are few positive clues as to the nature of the side chain-backbone hydrogen bonding patterns, and so a rather poorly ordered arrangement of the side chains is indicated.

A second distinct helical region is seen in the C-terminal portion of the peptide, extending from Pro^{14} to Lys^{24}. This helical domain is formed independently of the other structures seen in the peptide. The characteristic NOEs present are: $d_{\alpha N}(i,i+3)$ for residues Pro^{14}–Val^{17}, Trp^{15}–Gly^{18} (present but weak in the NOESY spectra with 200 ms of mixing time, absent at 100 ms), Val^{17}–Trp^{20}, Gly^{18}-Asp^{21} (weaker), Trp^{19}–Gln^{22}, and Asp^{21}–Lys^{24}, and $d_{\alpha\beta}(i,i+3)$ NOEs are seen for residues Pro^{14}–Val^{17}, Val^{17}–Trp^{20}, Gly^{18}–Asp^{21}, and Asp^{21}–Lys^{24}. Although a significant number of the NOEs expected in a classical α-helix were observed, the pattern of connectivities over this region was incomplete. For example, for residues Trp^{15} and Leu^{16}, the α-helical backbone NOEs are either absent or very weak. In addition, from a comparison of the strengths of $d_{NN}(i,i+1)$ NOEs with those in the N-terminal domain, it is apparent that the α-helical tendency is weaker in this C-terminal region. In a similar fashion, the reduction in backbone amide exchange rates was much less pronounced than in the N-terminal helix, so that although hydrogen bonding is present (*e.g.*, $Leu^{16}{}_{C=O}$–$Trp^{20}{}_{HN}$ and $Asp^{21}{}_{C=O}$–$Lys^{24}{}_{HN}$), it is relatively weak in the C-terminal region. As a consequence, the helical structure calculated in this area has a somewhat distorted backbone. However, this is not to say that the conformation in this area is poorly defined. The segment of the peptide between residues Pro^{14}–Trp^{20} is composed principally of large hydrophobic residues forming a distinct, compact hydrophobic

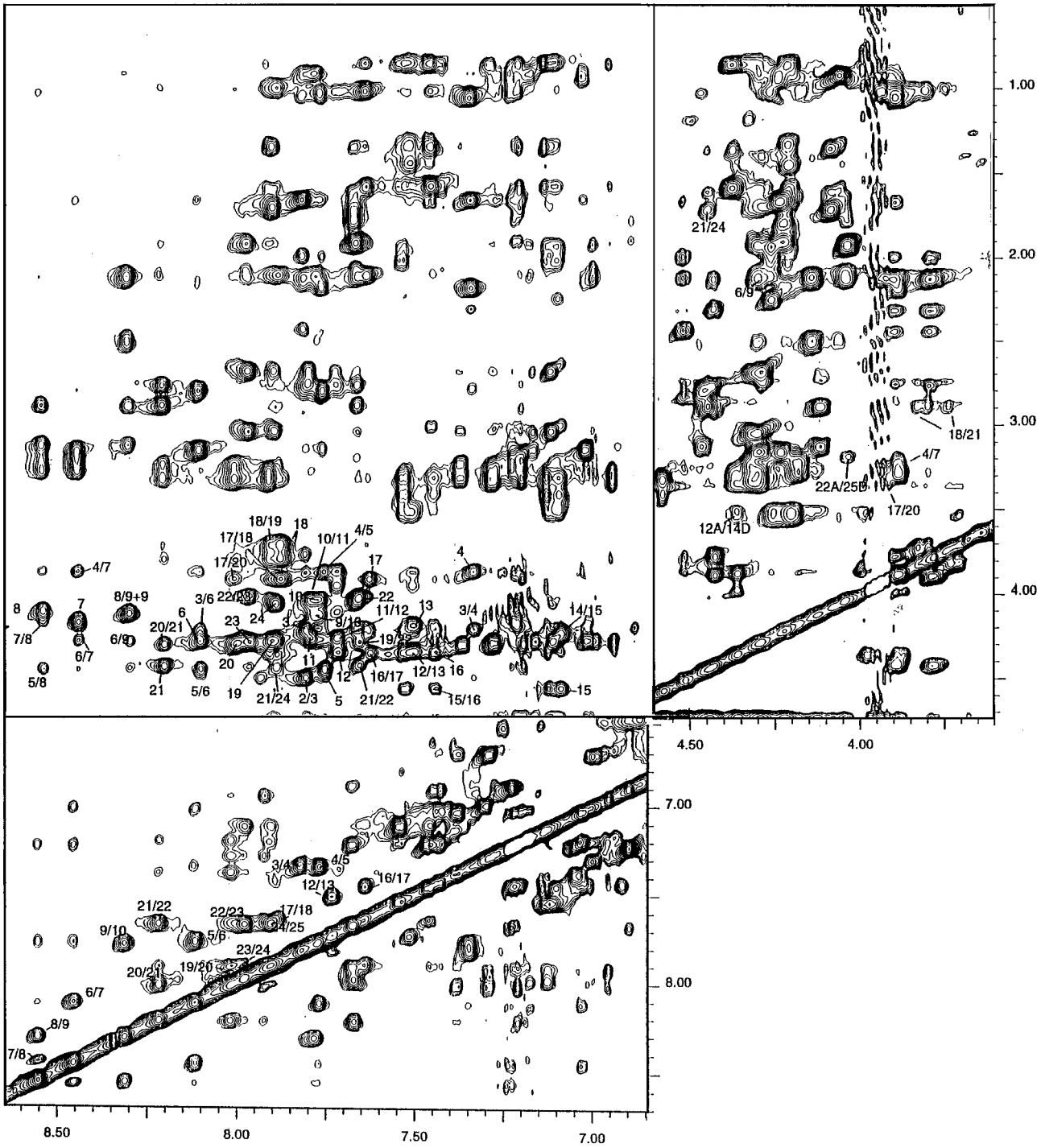

FIG. 1. **Sections from NOESY spectra.** Sections from the NOESY spectrum (200 ms of mixing time) were collected in 50% TFE/50% H_2O (v/v), pH 3.9. NOEs corresponding to connectivities within a single residue are labeled with a single number (*e.g.*, 15 refers to an NOE within residue Trp^{15}). Inter-residue connectivities are labeled with both residue numbers. In the *upper left panel* (amide to side chain and a connectivities), all dαN(i,i+1) and some long-range daN(i,i+3) connectivities are labeled. All sequential dNN(i,i+1) NOEs are labeled in the *lower panel*. The *upper right panel* shows the αH to side chain region in which some d$\alpha\beta$(i,i+3) and other medium range NOEs are labeled.

cluster (see Fig. 4). The conformation of this region is defined largely by the numerous NOEs between these side chains. Because the region is helical, many of these interactions are of the type i,i+3 and i,i+4 (summarized in Fig. 2; Refs. 31 and 32). It appears that the overcrowding of the bulky side chains in the cluster is a principal contributor to the distortion of this region away from regular α-helix. Thus the best description of the conformation over this section of the peptide is an irregular helix formed of multiple overlapping turns, defined in large part by side chain interactions. It should be noted that from the NOEs observed, the calculated structure may reflect a time averaged conformation for the peptide undergoing a dynamic transition between, for example, α- and 3_{10}-helix (*e.g.*, Refs. 33–35). Towards the C terminus of the peptide (residues 21–25), the regular pattern of α-helical NOEs is resumed with the calculated structure adopting that of a regular α-helix.

There are several noteworthy features in this C-terminal helix. Firstly, the presence of so many large hydrophobic residues over the region Pro^{14}–Trp^{20} in a helical conformation is relatively rare. However, other examples are known as can be

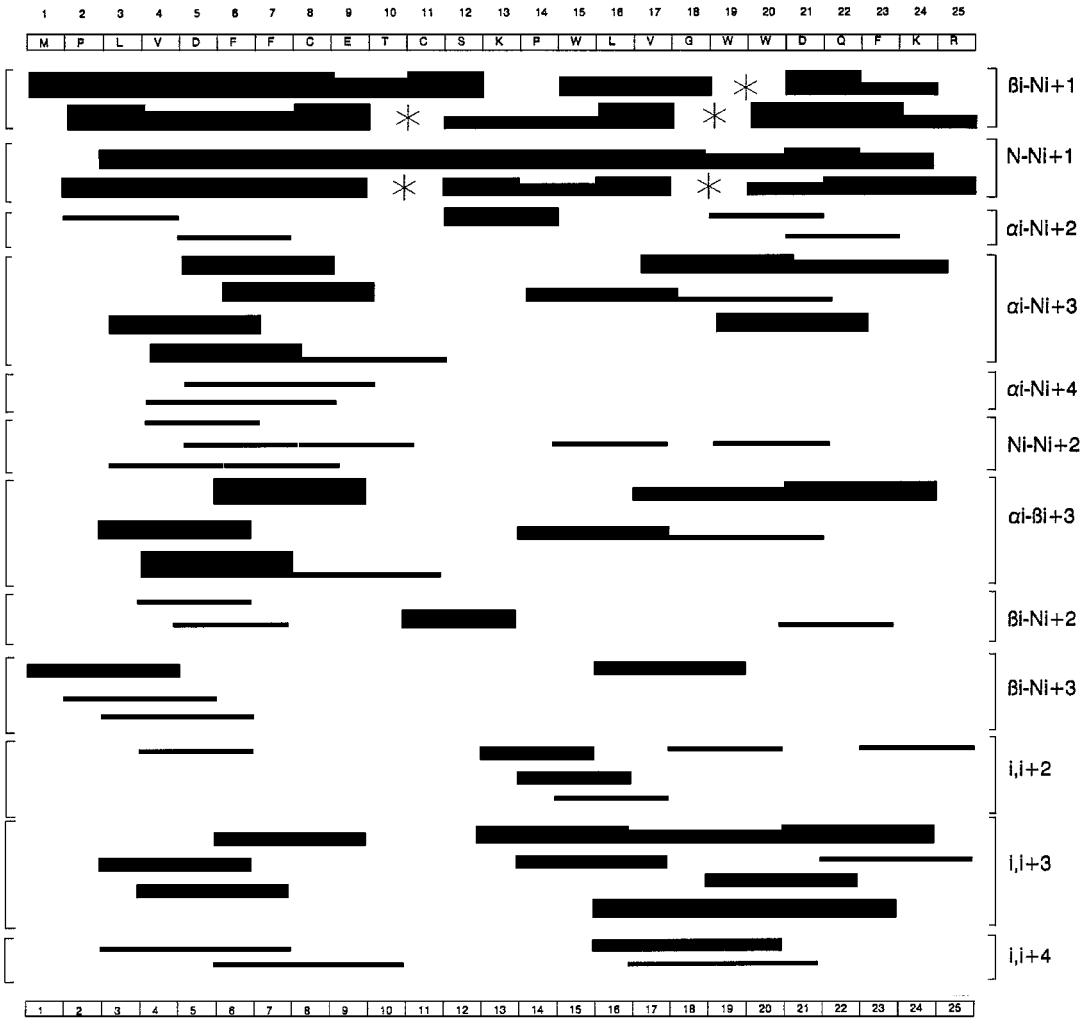

FIG. 2. **Summary of the NOEs observed for peptide 1-25 RD1.** An illustration of the sequential and medium range NOE connectivities for peptide 1-25 RD1 in 50% TFE/50% H_2O (v/v) is presented (composite of those observed at pH 3.9 and 6.0). The thickness of the bars reflects the intensities of the NOEs. The NOEs marked with *asterisks* could not be observed because of overlap of chemical shifts. The NOEs (*i*, *i*+2), (*i*,*i*+3), and (*i*,*i*+4) are those not part of the other illustrated classes, for example, the connectivity (*i*,*i*+2) indicates a class other than dαN(*i*,*i*+2), dNN(*i*,*i*+2), or dβN(*i*,*i*+2). For proline the δCH2 protons substitute for the NH protons. Greater than 95% of proline (residues Pro^2 and Pro^{14}) adopts a trans peptide backbone conformation.

seen, for example, in the helix 77–94 of actin (36). The initiation of the C-terminal helix we describe in this study appears to be associated with Pro^{14}, and in this regard, the involvement of proline in the first turn of an α-helix is well known (37). However, the orientation of the side chains of residues Pro^{14} and Trp^{15} is unusual. There are strong inter-residue NOEs, indicating numerous close contacts between the "stacked" flat surfaces of the rings. Over the rest of the hydrophobic cluster the distribution of the side chains is also distorted, as compared with the ideal α-helix, so that the large tryptophan rings, in particular, spread out more uniformly around the helical cylinder than might normally be expected and, in addition, lie closer to the peptide backbone in a position in which they become more protected from the solvent. As a consequence, there is an especially large number of *i*,*i*+3 NOEs in this hydrophobic domain, as compared with the *i*,*i*+4 side chain connectivities, which are most common in regular α-helix (see Fig. 2). There are numerous NOEs to the side chain of Leu^{16}, which forms interactions with the side chains of all three tryptophan residues 15, 19, and 20, making it the central residue in a highly distinctive hydrophobic patch. In contrast, the side chain of residue Val^{17} has many fewer connectivities and lies relatively exposed, pointing out from the opposite "face" of the peptide, forming a second possible site for specific interactions. The α-helical backbone NOEs are disrupted for residues Trp^{15} and Leu^{16}, and the helical NOEs $d_{a\beta}(i,i+3)$ are absent for residues Leu^{16}–Trp^{19}. This, together with the protection of the amide protons in this area from solvent exchange, means that the hydrogen bonding is weak. Consequently, there is a considerable disruption of the helical backbone in this domain and, in particular, the backbone dihedral angles for both Val^{17} and Gly^{18} lie outside the most favored region for regular α-helix in the Ramachandran plot. This disruption corresponds to a degree of conformational freedom around residues Val^{17}–Gly^{18} presumably arising from the cumulative difficulty of accommodating the tightly packed side chains (especially that of Val^{17}, which is branched close to the backbone at Cβ), and also the small size of Gly^{18}, which provides some space for movement. This conformational freedom around Val^{17}–Gly^{18} serves to separate residues of this compact, hydrophobic domain from the residues C-terminal to Gln^{22}.

In small helices, interactions at the termini are a substantial source of stability, and for the C-terminal helix, there appear to be several stabilizing interactions with residues Lys^{24} and Arg^{25}. Firstly, there will be a favorable interaction of two positively charged side chains with the helix dipole. In addition, an ion pair interaction Asp^{21}–Lys^{24} is indicated by the NOEs $Asp^{21}{}_{H\alpha}$–Lys^{24}(HN, Hγ, and H_β). It also appears that the

FIG. 3. **The calculated structure for the 1-25 RD1 peptide.** The figure shows six overlaid structures for the peptide 1-25 RD1. In the *lower pair* of structures, only the α-carbon atoms are shown. In the *upper pair* of structures, both backbone atoms, and side chains, either for residues Pro^{2}–Thr^{10} (*left*) or for residues Pro^{14}–Lys^{24} (*right*) are shown (no hydrogen atoms). On the *left-hand side*, alignment was made only for residues Pro^{2}–Thr^{10}, and on the *right-hand side* only the residues $Pro1^{4}$–Lys^{24} were aligned. An arbitrary color scheme is used: *yellow*, Pro^{2}, Cys^{8}, Pro^{14}, Trp^{19}, and Gln^{22}; *purple*, Leu^{3} and Leu^{16}; *green*, Val^{4}, Phe^{7}, Val^{17}, and Phe^{23}; *red*, Asp^{5}, Phe^{6}, Trp^{15}, Trp^{20}, and Asp^{21}; *pink*, Glu^{9}; *white*, Thr^{10} and Gly^{18}; *blue*, Lys^{24}.

residue Arg^{25} adopts the role of a C-cap, stabilizing the final turn of the helix by the formation of a hydrogen bond between the arginine side chain and the C=O of Gln^{22} (NOEs: $Gln^{22}{}_{H\alpha}$–$Arg^{25}{}_{H\delta}$ and a very weak $^{22}Gln_{HN}$–$Arg^{25}{}_{H\delta}$; see Ref. 35).

Deletion Analysis of RD1-CAT Chimera Used to Identify the Membrane Association Domain—^{1}H NMR structure determination of the N-terminal splice region of RD1 has thus identified two distinct helical structures separated by a mobile hinge region. That such discreet, self-folding domains are apparent in this peptide gives support to our contention that this splice region has distinct functional properties (9, 12, 19, 20, 38). These include an ability to attenuate the V_{max} of RD1 and to target RD1 exclusively to membranes. Furthermore, that this region can confer membrane association on chimeric species formed with the normally soluble enzyme CAT (12, 20) is consistent with this splice region being able to self-fold into a functional structure.

The structural analysis presented here, however, identifies distinct structural domains within this splice region, which encompasses two separate helical regions separated by a highly mobile hinge region. The first helical region comprises a well formed, amphipathic α-helix, whereas the second helical region contains a distinct, compact, highly hydrophobic domain (residues 14–20) having a distorted helical structure. This domain is rich in tryptophan residues and is highly ordered with many interactions occurring between the side chains. In order to address whether membrane association was attributable to one of these distinct structural domains, we undertook a deletion analysis. This was done using a chimera formed between an N-terminal region of RD1 fused, in-frame, to the N terminus of CAT (20). In this assay we generated mature radiolabeled chimera using an *in vitro* transcription/translational system. Such chimera were then incubated with membranes, and subsequently, a membrane pellet and supernatant fraction were isolated. From this it was possible to identify whether specific chimera became membrane-associated.

We have shown previously (20) that although CAT itself did not associate with membranes, 1-25 RD1-CAT did. Similarly, the chimera 1–100 RD1-CAT was membrane-associated, whereas the N-terminal truncated species, 26–100 RD1-CAT, which reflected deletion of the splice region, remained fully soluble (20). This exemplifies the importance of the first 25 amino acids of RD1 in conferring membrane association (9, 19, 20) and showed that the mere addition of extra N-terminal sequence to CAT, as in 26–100 RD1-CAT, was insufficient to elicit membrane association. The presence of sub-optimal Kozak sequences, preceding Met^{26} and Met^{37}, also allowed for the generation of the N-terminal truncated species 26–100 RD1 and, to a lesser extent, 37–100 RD1 in the *in vitro* synthesis system (20). These N-terminal truncated species did not become associated with membranes, thus providing internal controls in the association assay (20).

Four truncations were selected to probe functional attributes. These were (i) deletion of the hydrophobic region of the N-terminal, amphipathic α-helical domain (residues 2–7), (ii) deletion of the polar region of this amphipathic α-helical domain together with the hinge region (residues 8–13), (iii) deletion of the compact, hydrophobic, tryptophan-rich domain formed within the second helical region (residues 14–20), and (iv) deletion of the polar end of the second helical region (resi-

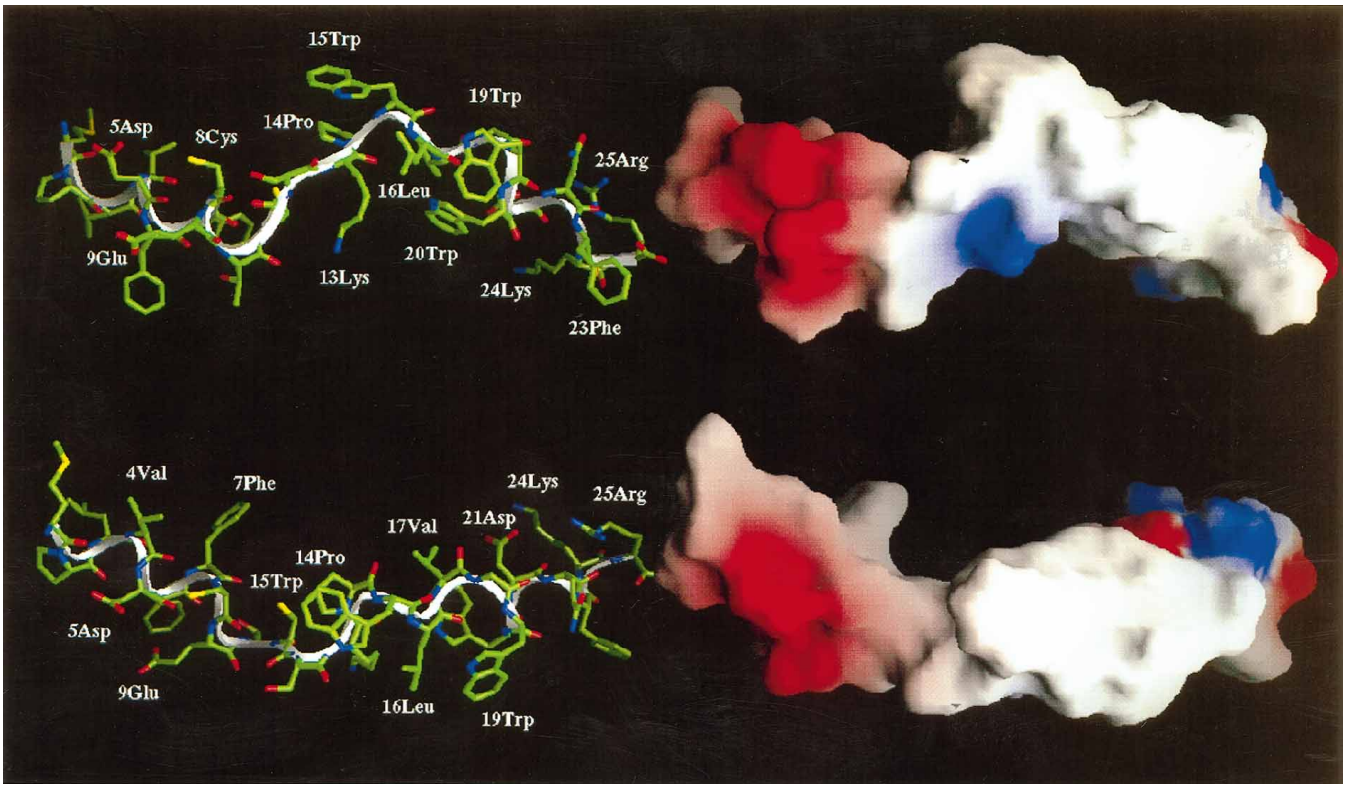

FIG. 4. **The mean calculated structure for peptide 1-25 RD1.** The figure shows two orientations of the average calculated structure for peptide 1-25 RD1. On the *left-hand side*, both backbone and side chain atoms are shown (no hydrogen atoms) for all residues. The helical path of the backbone is emphasized by the *white ribbon*. Certain residues are labeled. On the *right-hand side*, molecular surface maps are shown in the corresponding orientations. The surface is colored according to charge (*red*, negative; *blue*, positive). It is clear that the residues responsible for biological activity (Pro^{14}–Trp^{20}) form a hydrophobic cluster (*white*), flanked on either side by charged residues.

dues 21–25). Using this system we showed that as before (20), the 1–100 RD1-CAT expressing plasmid generated two major species representing 1–100 RD1-CAT and 26–100 RD1-CAT, of which only the full-length 1–100 RD1-CAT became membrane-associated (Fig. 5).

Deletions in the splice region of RD1 were then made using the primer pairs detailed in the Methods section. Analysis (Fig. 5*a*) of mature chimeric proteins containing the deletions ΔPro^{2}--Phe^{7} (ΔP2-F7), ΔCys^{8}–Lys^{13} (ΔC8-K13), and ΔAsp^{21}–Arg^{25} (ΔD21-R25) showed that these all became membrane-associated. In marked contrast to this, the mutant chimera expressing the deletion ΔPro^{14}–Trp^{20} (ΔP14-W20) was unable to become membrane-associated (Fig. 5). This suggests that the information that is critical for membrane association lies within this compact, highly hydrophobic, tryptophan-rich domain.

In all these constructs, save that for the ΔAsp^{21}--Arg^{25} deletion, an additional species, Met^{26-100} RD1CAT, was formed and observed as a faster migrating species upon electrophoresis (Fig. 5*a*). We have postulated (9, 12, 20) that Met^{26-100} RD1-CAT was generated as a result of the presence of a sub-optimal Kozak sequence (39) preceding Met^{26}, producing an N-terminal truncated species. This sub-optimal Kozak sequence (AGGATGG) (39) preceded Met^{26} in all of these RD1-CAT chimera save that of the ΔAsp^{21}–Arg^{25} deletion where it was destroyed upon engineering this particular deletion through the removal of the 15 nucleotides directly upstream of Met^{26}. However, there is a further sub-optimal Kozak sequence found in these chimeric species, namely one that would be predicted to generate Met^{37-100} RD1-CAT and whose production we have noted previously, albeit to a lesser extent than for Met^{26-100} RD1-CAT (20). In our studies on the ΔAsp^{21}–Arg^{25} deletion, we also observed the production of soluble species (Fig. 5*a*), which migrated on SDS-polyacrylamide gel electrophoresis at a position consistent (20) with that expected for Met^{37-100} RD1-CAT. Presumably the production of the N-terminal truncate occurred through transcriptional starts occurring at Met^{37} in RD1.

^{1}H NMR analysis showed that the stretch of amino acids given by Pro^{14}–Trp^{19} forms a discrete, compact domain that is stabilized by hydrogen bonding and Van der Waals interactions. This is, however, an intensely hydrophobic domain. Thus, in order to investigate whether membrane association was a function of the hydrophobicity of this domain per se, we replaced residues Pro^{14}–Trp^{20} with a "cassette" of seven alanine residues. Expression of this mutant chimera showed, however, that it failed to become membrane-associated (Fig. 5*b*). Thus the ability of RD1 to become membrane-associated is not due to a nonspecific hydrophobic interaction at this point within the splice region. Rather, it would appear to be determined by the unique structural properties of this tryptophan-rich domain bound by Pro^{14}–Trp^{20}.

Conclusions—All four PDE4 genes encode multiple splice variants, due to 5′ domain swapping, yielding proteins with distinct N-terminal regions (4, 11, 17, 18, 40). This study provides the first structural analysis of a splice region of a cyclic nucleotide phosphodiesterase. We show here that the N-terminal splice region of RD1 forms a distinct structure provided by two independently folding, helical regions separated by a mobile hinge region. That such a relatively small region should have such a distinct structure is consistent with it exhibiting particular biological properties, namely conferring absolute membrane association on RD1 and attenuating the catalytic activity of this enzyme (9, 12, 19). Structural studies, coupled with deletion analyses, have now allowed us to identify the domain with this N-terminal splice region, which confers membrane targeting upon RD1. This is a well defined, compact,

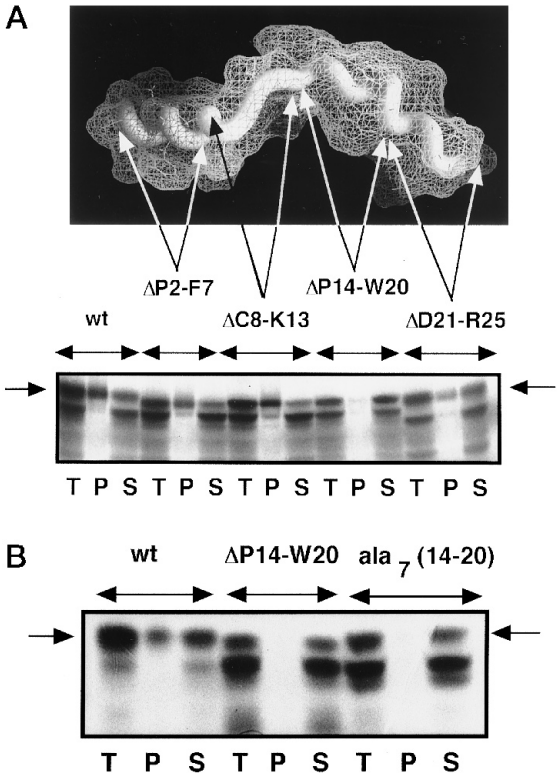

FIG. 5. **Analysis of the ability of mutant RD1-CAT chimera to become membrane-associated.** The plasmids generated in this study were used to prime a coupled transcription/translation system to produce mature chimeric CAT species in an *in vitro* system. This was done in the presence of [^{35}S]methionine to produce radioactive products as described in Ref. 20. After transcription/translation, a portion of the products of the reaction was kept for analysis, and the rest was incubated with COS cell membranes as described under "Materials and Methods." After this incubation, a high speed supernatant (soluble) fraction and a membrane fraction were isolated. These two fractions and that of the original product of the transcription/translation reaction were subjected to SDS-polyacrylamide gel electrophoresis. Identification of the various radioactive species was done using a PhosphorImager. Gel lanes were loaded such that the amount of the original transcription/translation product analyzed was identical to that found in the combined membrane and soluble lanes. Thus lanes analyzing particular plasmids can be compared directly. These studies utilize a chimeric species formed between the first 100 amino acids of RD1 and CAT. This species becomes membrane-associated in a similar fashion to that of the smaller chimera, 1-25 RD1-CAT (20). In *a* is shown a deletion analysis covering the indicated distinct structural regions of 1-25RD1 (*upper panel*) as regards the ability of these various mutant RD1-CAT chimera to become membrane-associated. The lanes are in sets of three, where tracks labeled *T* represent the original transcription/translation product, those labeled *P* represent the amount that can become pellet-associated, and those labeled *S* represent that which remained soluble. Data are shown for the native chimera of 1–100RD1-CAT (*wt*) together with the indicated mutant chimera that exhibit specific deletions at residues 2–7RD1 (ΔP2-F7), residues 8–13RD1 (ΔC8-K13), residues 14–20RD1 (ΔP14-W20), and residues 21-25RD1 (ΔD21-R25). The slowest moving band, indicated with the *arrow*, in each of these sets represents the chimeric species stated above. The faster moving species, for all except the ΔD21-R25 deletion, as discussed in some detail before (20), correlates with the truncate 26–100RD1 formed due to a suboptimal Kozak sequence that precedes Met^{26}. This, however, is disrupted in the DD21-R25 mutant, and the faster running species correlates with 37–100RD1-CAT, which also exhibits a sub-optimal Kozak sequence (20). These N-terminal truncated species produced in each case do not include the N-terminal membrane targeting splice region of RD1, are found exclusively as soluble species, and serve as internal controls (the radioactivity seen in the S fraction for these species is identical to that seen in the T fraction). In *b* is shown data for a mutant 1–100RD1-CAT chimera, where residues 14–20RD1 were replaced by a cassette of seven alanine residues (*ala$_7$(14–20)*). The ability of this species to become membrane-associated was compared with 1–100RD1-CAT (*wt*) and the deletion chimera which lacked residues 14–20RD1 (ΔP14-W20). Studies were done as described above. These data are typical of an experiment done three times.

intensely hydrophobic domain encompassing residues Pro^{14}–Trp^{20}. It is, however, difficult to see how this tryptophan-rich region could insert directly into a membrane bilayer, and thus we consider it much more likely that membrane association is conferred through protein-protein interaction between RD1 and a membrane "anchor" protein. Such an interaction might offer an explanation for our observations that RD1 exhibits a distinct subcellular distribution in both brain and transiently transfected COS cells (9, 19), where it is found associated with both plasma membrane and Golgi fractions, and also in stably transfected human thyroid carcinoma cells, where it is expressed uniquely in the Golgi.[2] For, if RD1 was able to insert generally into lipid bilayers, then one might expect this PDE to have been distributed nonspecifically among all intracellular membranes. The presumptive membrane protein anchor that interacts with this domain of RD1 is unknown. However, the means of interaction, although likely to be intensely hydrophobic in nature, is clearly not nonspecific as replacement of the targeting domain formed by Pro^{14}–Trp^{20} with a cassette of seven alanine residues failed to allow for membrane association. Thus distinct structural features of this domain of RD1 appear to be required for membrane association to occur. Nevertheless, the underlying hydrophobic basis of such an interaction may explain why it seemingly can be disrupted by very low levels of detergent (9, 19, 20) and, because it is likely to be of high affinity, would explain why all observable RD1 is membrane-associated in brain and in transfected COS cells (12) and transfected thyroid cells.[2]

Acknowledgments—We thank the Medical Research Council for financial support and the Wellcome Trust and Scottish Home and Health Department for equipment grants. We thank The Wellcome Trust for financial support and A. J. Pemberton for maintaining the NMR facilities. We thank Dr. James Milner-White for helpful discussions. Further details and illustrations relevant to this study appear on a WWW page (http://www.ibls.gla.ac.uk/IBLS/Staff/m-houslay/HouslayLab.html).

REFERENCES

1. Krebs, E. G., and Beavo, J. A. (1979) *Annu. Rev. Biochem.* **43,** 923–959
2. Beavo, J. A., Conti, M., and Heaslip, R. J. (1994) *Mol. Pharmacol.* **46,** 399–405
3. Manganiello, V. C., Murata, T., Taira, M., Belfrage, P., and Degerman, E. (1995) *Arch. Biochem. Biophys.* **322,** 1–13
4. Conti, M., Nemoz, G., Sette, C., and Vicini, E. (1995) *Endocr. Rev.* **16,** 370–389
5. Rubin, C. S. (1994) *Biochim. Biophys. Acta* **1224,** 467–479
6. Scott, J. D. (1991) *Pharmacol. & Ther.* **50,** 123–145
7. Klauck, T. M., and Scott, J. D. (1995) *Cell. Signalling* **7,** 747–757
8. Houslay, M. D., and Kilgour, E. (1990) (Beavo, J. A., and Houslay, M. D., eds) *Molecular Pharmacology of Cell Regulation,* Vol. 2, pp. 185–226, John Wiley & Sons Ltd., Chichester, UK
9. Shakur, Y., Pryde, J. G., and Houslay, M. D. (1993) *Biochem. J.* **292,** 677–686
10. Houslay, M. D., and Marchmont, R. J. (1981) *Biochem. J.* **198,** 703–706
11. Bolger, G., McPhee, I., and Houslay, M. D. (1996) *J. Biol. Chem.* **271,** 1065–1071
12. McPhee, I., Pooley, L., Lobban, M., Bolger, G., and Houslay, M. D. (1995) *Biochem. J.* **310,** 965–974
13. Horton, Y. M., Sullivan, M., and Houslay, M. D. (1995) *Biochem. J.* **308,** 683–691
14. Milatovich, A., Bolger, G., Michaeli, T., and Francke, U. (1994) *Somatic Cell Mol. Genet.* **20,** 75–86
15. Szpirer, C., Szpirer, J., Riviere, M., Swinnen, J., Vicini, E., and Conti, M. (1995) *Cytogenet. Cell Genet.* **69,** 11–14
16. Swinnen, J. V., Joseph, D. R., and Conti, M. (1989) *Proc. Natl. Acad. Sci. U. S. A.* **86,** 5325–5329
17. Bolger, G. (1994) *Cell. Signalling* **6,** 851–859
18. Davis, R. L., Takayasu, H., Eberwine, M., and Myres, J. (1989) *Proc. Natl. Acad. Sci. U. S. A.* **86,** 3604–3608
19. Shakur, Y., Wilson, M., Pooley, L., Lobban, M., Griffiths, S. L., Campbell, A. M., Beattie, J., Daly, C., and Houslay, M. D. (1995) *Biochem. J.* **306,** 801–809
20. Scotland, G., and Houslay, M. D. (1995) *Biochem. J.* **308,** 673–681
21. Sheffield, V. C., Cox, D. R., Lerman, L. S., and Myers, R. M. (1989) *Proc. Natl. Acad. Sci. U. S. A.* **86,** 232–236
22. Brunger, A. T. (1992) X-PLOR, version 3.1, *A System for X-ray Crystallography and NMR,* President and Fellows of Harvard University, Yale University Press, Cambridge, MA

[2] L. Pooley, Y. Shakur, G. Rena, and M. D. Houslay, submitted for publication.

23. Lau, S. Y. M., Taneja, A. K., and Hodges, R. S. (1984) *J. Biol. Chem.* **259,** 13253–13261
24. Dyson, H. J., Merutka, G., Waltho, J. P., Lerner, R. A., and Wright, P. E. (1992) *J. Mol. Biol.* **226,** 795–817
25. Nelson, J. W., and Kallenbach, N. R. (1989) *Biochemistry* **28,** 5256–5261
26. Ho, S. N., Hunt, H. D., Horton, R. M., Pullen, J. K., and Pease, L. R. (1989) *Gene* (*Amst.*) **44,** 51–59
27. Dyson, H. J., Rance, M., Houghten, R. A., Lerner, R. A., and Wright, P. E. (1988) *J. Mol. Biol.* **201,** 161–200
28. Hol, W. G. J., van Duijenen, P. T., and Berendsen, H. J. C. (1978) *Nature* **273,** 443–446
29. Sali, D., Bycroft, M., and Fersht, A. R. (1988) *Nature* **335,** 740–743
30. Richardson, J. S., and Richardson, D. C. (1988) *Proteins Struct. Funct. Genet.* **4,** 229–239
31. Scholtz, J. M., Qian, H., Robbins, V. H., and Baldwin, R. L. (1993) *Biochemistry* **32,** 9668–9676
32. Shoemaker, K. R., Kim, P. S., York, E. J., Stewart, J. M., and Baldwin, R. L. (1990) *Nature* **326,** 563–567
33. Tirado-Rives, J., and Jorgensen, W. L. (1991) *Biochemistry* **30,** 3864–3871
34. Fiori, W. R., Lundberg, K. M., and Millhauser, G. L. (1994) *Nat. Struct. Biol.* **1,** 374–377
35. Fiori, W. R., and Millhauser, G. L. (1995) *Biopolymers* **37,** 243–250
36. Kabsch, W., Mannherz, H. G., Suck, D., Pai, E. F., and Holmes, K. C. (1990) *Nature* **347,** 37–44
37. MacArthur, M. W., and Thornton, J. M. (1991) *J. Mol. Biol.* **218,** 397–412
38. Houslay, M. D., Scotland, G., Pooley, L., Spence, S., Wilkinson, I., McCallum, F., Julien, P., Rena, N. G., Michie, A. M., Erdogan, S., Zeng, L., Oconnell, J. C., Tobias, E. S., and MacPhee, I. (1995) *Biochem. Soc. Trans.* **23,** 393–398
39. Kozak, M. (1986) *Cell* **44,** 283–292
40. Conti, M., Swinnen, J. V., Tsikalas, K. E., and Jin, S. L. C. (1992) in *Advances in Second Messenger & Phosphoprotein Research* (Strade, S. J., and Hikaka, H., eds) Vol. 25, pp. 87–99, Raven Press, Ltd., New York